Int. J. Multiphase Flow Vol. 18, No. 2, pp. 159–179, 1992
Printed in Great Britain

0301-9322/92 $5.00 + 0.00
Pergamon Press plc

CHARACTERISTICS OF THE SPRAY FROM A DIESEL INJECTOR

Y. HARDALUPAS, A. M. K. P. TAYLOR and J. H. WHITELAW
Imperial College of Science, Technology and Medicine, Mechanical Engineering Department, London SW7 2AZ, England

(Received 1 March 1991; in revised form 15 October 1991)

Abstract—Spatial and temporal profiles of the velocity of the entrained air and 60 and 30 μm droplets, together with the associated fluxes, from a 5-hole diesel spray exhausting into atmosphere at a repetition rate of 10 Hz have been measured with a phase-Doppler anemometer. The nozzle diameters, fuel charge per hole, injection duration and the area-averaged spray velocity during this duration were 0.18 mm, 2.35 mm^3, 0.7 ms and $U_0 = 132$ m/s, respectively. The Sauter mean diameter of the fuel droplets decreased from a maximum centreline value of around 80 μm at 100 diameters from the nozzle to 38 μm at 780 diameters, and a similar decrease was observed between 1 and 2 ms after the start of injection at the upstream location. The flux carried by the 30 μm droplets was up to twice that associated with the 60 μm droplets, 2 ms after injection, although the velocities of the larger droplets were consistently higher than those of the smaller droplets. The maximum measured ensemble-averaged relative velocity was 0.45 U_0 for 60 μm droplets just after the arrival of the spray at 550 diameters from the nozzle. The magnitudes of the Weber number imply that droplet breakup was always confined to the leading edge of the spray and was limited to, at most, the initial 1/2 ms of the passage of the spray past a given point. Breakup was mostly complete by 550 diameters from the nozzle. Thus, the measured decrease in the mean diameter was due to small droplets, generated by breakup at the leading edge of the spray, losing velocity due to aerodynamic drag and falling behind the leading edge. Droplets generated late in the injection schedule were likely to overtake those generated earlier and together with the fan-spreading effect, which arises from the combination of the root mean square (RMS) droplet radial velocity and the radial profile of the ensemble-averaged droplet axial velocity, led to RMS velocities in the axial component of the droplets that were not associated with the transfer of turbulent motion from the air.

Key Words: phase-Doppler anemometer droplet size and velocity correlation, droplet flux, atomization, breakup

1. INTRODUCTION

The sprays of diesel engines are known to travel large distances with low spreading rates and atomization is often due to impingement on the piston crown. Because of the high velocities, short injection durations and the density of the liquid, measurements of droplet diameter, flux and particularly relative velocity are not available in sufficient detail to quantify the characteristics of the spray as it develops in time and distance and to identify the spatial extent over which atomization occurs in the spray. A major reason for this situation is the limitations imposed by measuring techniques.

In general, it is necessary to use optical methods to measure droplet properties and descriptions of the initial breakup of the liquid core have been provided by laser-sheet photography (e.g. Felton *et al.* 1987; Yule & Aval 1989; Arcoumanis *et al.* 1990a, b) and associated image processing (e.g. Shimizu & Emori 1987). Other gross features of the spray, such as tip velocity and penetration rates, have also been measured (e.g. Yule *et al.* 1985; Arai *et al.* 1985). Measurements of size have been made by instruments based on the Fraunhofer diffraction of a laser beam (e.g. Nakayama 1987; Tamata *et al.* 1985), although the results are averages over the length of a typically 9 mm dia beam. Measurements of the velocity characteristics of diesel sprays have been obtained with good spatial resolution using laser-Doppler anemometry in atmospheric pressure environments (Wu *et al.* 1984; Obokata *et al.* 1988) and in engine conditions (Saffman *et al.* 1988), but without corresponding simultaneous information about the diameter. As a consequence of these investigations, it is known that initial velocities can exceed 200 m/s and decay rapidly, that spreading angles are of the order of 10° and the unconnected liquid structures exist after 50 diameters with decreasing size thereafter (Cavaliere *et al.* 1988). There are, however, many unknowns, including the magnitudes of the velocity of the entrained air and of the relative velocity between the droplets and air as a function of the droplet size, a quantity which controls the Weber number and hence where breakup occurs,

the spatial distribution of the mean diameter across the spray and the relative magnitude of the flux carried by each droplet size class, where the mean is obtained from an ensemble-averaging process. Many authors have presented the variation of the mean diameters within these sprays because of the practical importance of these quantities. Flux measurements have been less widely reported, presumably because extinction of the beam is known to be strong in these sprays. It is important to realize, however, that with any single-particle counter, such as the phase-Doppler anemometer, the presentation of mean diameters is implicitly based on the flux measurement and, recognizing this, we have chosen to present some flux measurements in addition to the profiles of mean diameters. Our justification is presented below. These unknowns would be removed by simultaneous measurement of droplet velocity and size, and hence would permit the assessment of mathematical models of droplet breakup and coalescence.

In principle, the amplitude of Doppler signals can be interpreted in terms of droplet size and correlated with droplet velocity, as by Maeda *et al.* (1988), but the results can be ambiguous for a number of reasons including the effects of multiple scattering investigated by Kliafas *et al.* (1985, 1990). As a consequence, Maeda *et al.* (1988) report velocities for droplets below 15 μm and above 50 μm. An alternative approach is to use phase-Doppler anemometry which is, as shown by Hardalupas *et al.* (1988), less susceptible to the effects of multiple scattering than is the amplitude-based instrument. The phase-Doppler anemometer can also provide information of the quantity of fluid in given droplet-size ranges as shown by Hardalupas *et al.* (1990a, b) in kerosene and gasoline sprays, respectively. Recently, detailed measurements of diesel spray velocity correlated with size and with high temporal and spatial resolution have been made using phase-Doppler anemometry for a diesel spray injecting into the ambient atmosphere by Koo & Martin (1990) and by Pitcher & Wigley (1989). The results of Koo & Martin (1990) show that the largest velocity and diameter occur on the axis of the spray and quantify the acceleration of the entrained air near the injector tip at the start of injection. However, it is difficult to estimate the magnitude of the corresponding relative velocity between the droplets of a given diameter and the air, and hence to locate the areas in which breakup is likely to occur. Pitcher & Wigley (1989) present measurements of an alcohol spray in an engine at pressures up to 56 bar and the results highlight the limited extent of the liquid core and the small radial spread of the fuel droplets.

The present investigation provides measurements of droplet relative velocity and associated fuel flux as a function of time after injection and position downstream of the nozzle for a given volume of injected fuel. These two measurements are not presented in the otherwise comprehensive measurements of Koo & Martin (1990). In addition, the Sauter and arithmetic mean diameters are quantified. The commercial fuel injector was identical to that of Arcoumanis *et al.* (1990a) and sprayed into the ambient atmosphere.

The experimental arrangement, including the injector and phase-Doppler anemometer, are described in the following section which also indicates the uncertainties associated with the instrumentation. The results are presented in section 3 and the implications are discussed in section 4, particularly with respect to injection into environments typical of diesel engines. The paper ends with a summary of more important conclusions. The limitations of the measurement technique emerge in the presentation of the results and specific comments on its relative advantages are included in the discussion (section 4) and in the conclusions (section 5).

2. EXPERIMENTAL ARRANGEMENT

2.1. Injector

A 5-hole Bosch injector was used, inclined at 30° to the vertical, so that the spray from one hole was injected vertically downwards, while the fuel from the other holes was collected downstream of the nozzle using a special adaptor. Figure 1 shows a diagram of the atomizer. Each hole had a diameter $D = 0.18$ mm and length $L = 0.7$ mm, giving a ratio $L/D = 3.9$. The diesel fuel was supplied from a tank through a filter and a distributor-type pump using a high-pressure line 310 mm long and 1 mm i.d. The complete injection system was fixed on a traversing mechanism. The pump was driven by an electric motor at 600 rpm and established an injection frequency of 10 Hz, which corresponds to a four-stroke engine working at 1200 rpm. The rack of the pump was adjusted to

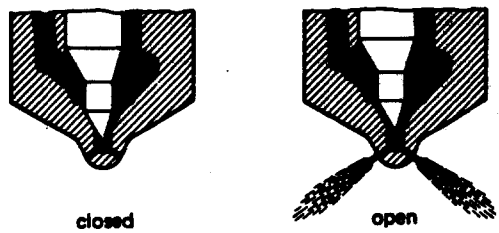

Figure 1. General arrangement of a Bosch multihole-type diesel injection nozzle (taken from Anon. 1971).

deliver a charge of 2.35 mm^3 per hole per injection and resulted in an injection duration of around 0.7 ms. At this speed, each millisecond corresponds to 7.2° of crank angle. The diesel fuel was Shell gas oil with density 844 kg/m^3 and kinematic viscosity 3.5×10^{-6} m^2/s at 40°C. The injected fuel was collected by an exhaust system equipped with a cyclone to separate liquid droplets from the air. The injector worked in an open atmosphere with the exhaust collection hood placed well downstream of the last measurement station. This arrangement ensured that the small drops from earlier injections were not re-injested by subsequent injections, but without having a large effect on the surrounding air flow.

Preliminary experiments using diesel fuel with red dye, which is added to distinguish grades of fuel which attract different tax, resulted in a reduced data rate and a larger proportion of measurements being rejected through failure to satisfy the "phase ratio" validation criterion (Hardalupas 1989), as compared to diesel fuel without dye, which is sold for automotive use. The dye had this effect because it absorbed some of the light refracted through the droplets and increased the amplitude of light scattered by reflection at the surface of the droplet relative to that refracted through the droplet. The dye-less fuel was therefore used for these experiments and resulted in a higher data rate. The refractive index was taken as 1.4, a value representative of multi-component fuel oil (Pitcher *et al.* 1990).

2.2. Phase-Doppler system

The phase-Doppler anemometer is an extension of the laser-Doppler anemometer, which measures simultaneously the size and velocity of individual spherical particles and the custom-built system described by Hardalupas (1989) was used here. An argon-ion laser was used and operated at 0.5 W and 514.4 nm wavelength. The collection angle used for the present applications was 30° off-axis in the forward direction, where refraction through the particle is the dominant light scattering mechanism. The optical characteristics and the sizing range of the system used in the applications is given in table 1. The calibration curve of the instrument depends on the relative refractive index, defined as the ratio of the refractive index of the material to that of the surrounding fluid, when refracted light through the droplets is mainly collected to get the sizing information. The change of the relative refractive index if the surroundings are fuel vapour, instead of air, is $\ll 1\%$ and has practically no effect on the accuracy of the sizing measurements (Hardalupas 1989).

The Doppler frequency and phase difference, between three photodetectors, were measured by a custom-built zero-crossing counter processor based on a 500 MHz clock. The Doppler bursts were required to have a minimum of 10 cycles above a threshold and the same frequency over the first 5 and 8 cycles within a small (1.5%) percentage tolerance. Two ratios, formed from the three measured phase differences, were required to fall within user-specified tolerances of a value derived from light scattering theory (Hardalupas 1989). The clock gave rise to uncertainties in the Doppler frequency of $< 1\%$ and in the phase measurement of $< 10\%$ for sizes $> 15\,\mu m$. The maximum Doppler frequency that could be measured by the counter processor was 15 MHz, corresponding to 1.04 U_0, where $U_0 = 131.9$ m/s was the area-averaged spray velocity at the nozzle exit, calculated on the assumption that the fuel flow rate was constant during injection. The measurements were restricted to values of U, the ensemble-averaged axial velocity, defined below, $< \sim 0.5\ U_0$ to avoid truncation of the velocity probability distribution. This was because of the width of the distribution, as can be inferred from the large corresponding fluctuation intensities, u'/U, where u' is the root mean square (RMS) value of the fluctuations, which approached values of about 0.25. As a consequence, measurements at a distance of 20 mm from the nozzle were restricted to the tail-end

Table 1. Principal characteristics of the phase-Doppler anemometer for the diesel injector experiment

1W (nominal) Ar^+ laser operated at	0.7 W
	514.5 nm
Beam diameter of laser, at e^{-2} intensity	1.25 mm
Focal length of the lenses:	
imaging lens from laser to grating	80 mm
collimating lens after the grating	200 mm
imaging lens to form measuring volume	600 mm
Number of lines on radial diffraction grating	16,384
Frequency shift (nominal) due to rotation of the grating	1 MHz
Short term stability of frequency shift (RMS)	0.3%
Beam separation	35 mm
Measured half-angle of intersection	1.635 deg
Calculated dimensions of beam intersection volume at e^{-2} intensity	4.73 mm
	0.135 mm
	0.135 mm
Fringe spacing	9.016 μm
Calculated number of fringes within e^{-2} intensity	15
Frequency to velocity conversion factor	0.11 MHz/(m s^{-1})
Location of collection optics from forward scatter	30 deg
Focal length of collimating lens in receiving optics	600 mm
Apertures at collimating lens:	
dimension of rectangular apertures	45 × 6 mm
separation between apertures 1 and 2	25 mm
separation between apertures 1 and 3	50 mm
Focal length of imaging lens in receiving optics	300 mm
Width of spatial filter before the photodetectors	100 μm
Magnification of receiving optics	2
hence effective length of probe volume	200 μm
Phase-angle-to-diameter conversion factor between channels 1 and 3	0.436 μm/deg

of the spray cloud. Farther downstream, measurements extended into the main body of the spray cloud and those close to the leading edge of the spray, defined as the region when $\partial U/\partial t$ was positive, were possible from 550 nozzle diameters.

The counter-based processing system produced time-resolved measurements of the unsteady sprays from which ensemble-averages could be calculated of the velocity, $\langle U(t)\rangle$, or other quantities of interest, at a given time t after the beginning of injection, as follows:

$$U = \langle U(t)\rangle = Lt(1/N)\sum U(t),$$

where the limit is taken as N, the number of repeats of injection, tends to infinity and the summation is over a set of samples $U(t)$, each taken at time t after the beginning of one of a set of N repeats of injection. The counter was externally gated to measure over a time window of 0.5 ms by a TTL pulse train, which was obtained from the "delayed gate" output of an oscilloscope, synchronized with the injection pulse which was generated by the needle lift after calibration. The length of the window was a compromise between the requirements that it be much smaller than the injection duration and that statistically reliable averages should be arrived at within a practically convenient number of injections. It should be noted that it could take up to 45 min to collect 5000 measurements in the most dense region of the spray. The value of 0.5 ms resulted in some broadening of the RMS results. Experiments performed with a 0.25 ms window resulted in RMS velocity fluctuations which were reduced by around 10%, but unchanged ensemble-averaged velocities. The latter value is the expected magnitude of the uncertainty due to the collection over windows which are not small compared with the characteristic time of injection.

Data rates are higher for a laser-Doppler anemometer and this implies that many signals from the spray are rejected and, clearly, *absolute* flux measurements are not possible, at least in these regions. The *relative* flux measurement is likely to be less affected, as argued below, however.

The measurements were based on 5000 samples at each point, resulting in statistical uncertainties of $\pm 3\%$ in the ensemble average, $\pm 10\%$ in the RMS velocity and $\pm 2\%$ in the cumulative size distribution based on the number of droplets (Tate 1982). A referee has pointed out that the accuracy of the measurements is also a function of the decrease in the signal-to-noise ratio which occurs in this spray and which may result in a bias of both the velocity and size measurements,

particularly as the core region is approached. Additional research is required to account for this effect which we leave for future work.

The sizing information is presented in terms of the mean diameters defined as:

Sauter mean diameter (SMD),

$$d_{32} = \sum C_i d_i^3 \Big/ \sum C_i d_i^2 \qquad [1]$$

and

arithmetic mean diameter (AMD),

$$d_{10} = \sum C_i d_i \Big/ \sum C_i, \qquad [2]$$

where C_i is the ensemble-averaged number density (m^{-3}) of droplets of size i, which corresponds to the mean diameter d_i, measured at a given time after injection. In what follows, it is understood that the mean diameter refers to an ensemble-averaged quantity. The number density was calculated from measurements of droplet residence time, according to Hardalupas & Taylor (1989). The anemometer measured a temporal size distribution based on single particles (Bachalo *et al.* 1986) and this contains information of the local fuel flux, a conserved quantity in non-reacting flow. The spatial size distribution is also useful in combustion applications, where fuel ignition and burning are functions of droplet population within a given volume of space, and this was derived from the measured temporal size distributions according to the method suggested by Hardalupas & Taylor (1989). The SMD and AMD presented here are based on the spatial size distribution and the tolerances are estimated to be of the order of $\pm 10\%$ for both measurements.

3. RESULTS

In the following results, velocity was normalized by U_0, defined earlier, and radial and axial distances from the nozzle were normalized by the diameter of the nozzle, D.

Measurements of droplet velocity, size and flux were obtained at distances of 20, 40, 60, 80, 100 and 140 mm from the nozzle corresponding to $z/D = 110$, 220, 330, 440, 550 and 780 as a function of time after the beginning of injection. Those in the temporal profile were taken until there was no longer a large difference between the velocity of each size class; it should be noted that this was not the end of the passage of the spray cloud. The measurements extend further downstream than in an engine because much can be learnt about the initial spray from the development far downstream, where comprehensive measurements were not limited by extinction. Thus, although a major part of the injection core was not measured, the *results* of the atomization were. Hence, for example, mathematical models of atomization can be evaluated by comparing the numerical with the experimental results at the farthest downstream stations. The characteristics of the size ranges of 0–10, 20–30 and 50–60 μm droplets are presented in the following figures and are referred to in the text as 10, 30 and 60 μm droplets. The smallest size range was chosen to provide measurements which are expected to be close to those of the entrained air: justification is provided below for this statement. The largest class was the largest class for which statistically reliable averages, based on several hundred realizations, could be obtained conveniently and, as will be demonstrated below, the velocity of this size closely corresponds to the limit beyond which droplet breakup would be expected to exist. The 30 μm class was chosen to give an indication of the velocity of the modal diameter.

The ensemble-averaged axial velocity component of the 10, 30 and 60 μm droplets on the centreline as a function of time after the beginning of injection can be seen in figure 2. Figure 3 presents the RMS fluctuations of the axial and radial velocity, u' and v' respectively, at $z/D = 550$ and figure 4 shows the volume flux results for the same three size classes—presented to provide an indication of the relative contribution of the three size classes to the flow of diesel fuel. Figure 5 shows typical size distributions in the spray and these are conveniently summarized by the temporal variation of the SMD and the AMD, which are presented at different locations on the centreline in figure 6. These mean diameters provide a convenient quantification of the reduction in the mean

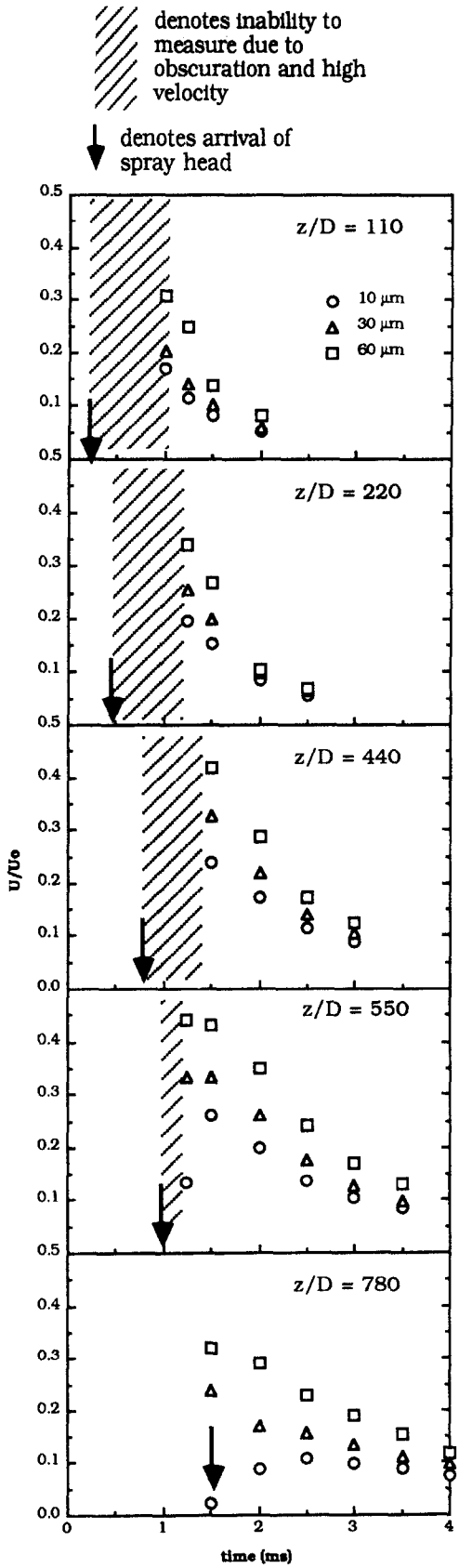

Figure 2. Temporal profiles of centreline ensemble-averaged axial velocity at $z/D = 110$, 220, 440, 550 and 780 for 10, 30 and 60 μm droplets.

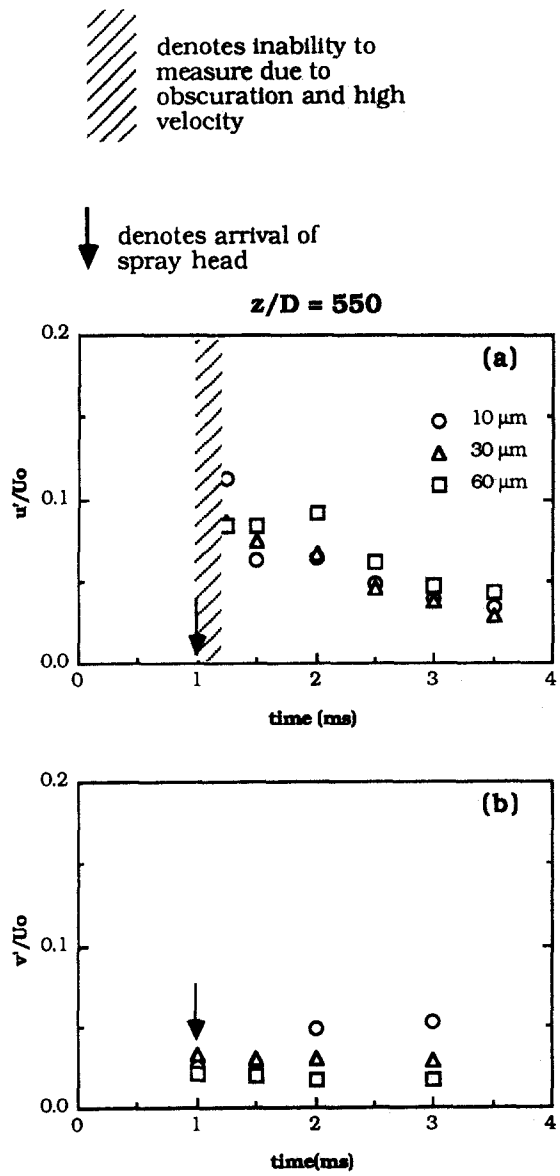

Figure 3. Temporal profiles of centreline values of the RMS of fluctuations of axial, u', and radial, v', velocity at $z/D = 550$ for 10, 30 and 60 μm droplets.

Table 2. Tip penetration of the diesel spray

Position z/D	Time (ms)
110	0.2
220	0.37
330	0.58
440	0.8
550	1.0
780	1.5

Table 3. Diesel spray droplets characteristics

Droplet dia (μm)	Relaxation time (ms)
10	0.26
30	2.25
60	8.9

diameter, which is the objective of the atomization process. The flux of the smallest diameters, below about 5 μm, is probably partly underestimated by the "roll-off" in the response of the instrument. The net effect of this size range on the mean diameter and flux characteristics of the spray is, however, small and the roll-off will not affect the measurements presented. In order to examine the development of the spray during its flight, the centreline characteristics at times 0.7 and 1.8 ms after the tip arrival at the measurement location are presented in figures 7 and 8 as spatial profiles. The radial profiles of the ensemble-averaged and RMS axial velocities, of the fluxes and the AMD and SMD of the droplets at $z/D = 110$, 550 and 780 for increasing times from the beginning of injection are shown in figures 9–12.

3.1. Temporal centreline characteristics

3.1.1. Velocity. Temporal variations of the ensemble-averaged axial velocity characteristics of the 10, 30 and 60 μm droplets are related to the time at which the spray tip arrives at each station with the values given in table 2. The delay between the arrival of the tip and the first measurable point of the temporal profile, figure 2, decreases with increasing distance from the injector as the velocities which occur progressively fall within the bandwidth of the counter. Thus, at $z/D = 780$, the spray velocity and density are sufficiently low for measurements to begin immediately on arrival of the first droplets, in the leading edge of the spray. At the other extreme, for $z/D = 110$, measurements begin at about 0.8 ms after tip arrival, or about 0.3 ms after injection has ceased, so that these correspond to the tail-end of the spray.

Table 3 gives the relaxation times of 10, 30 and 60 μm dia droplets, defined as the time required for a given diameter to decelerate to e^{-1} of the initial velocity difference between the droplet and surrounding constant velocity fluid, and calculated by the method of Fuchs (1964). The relaxation time of a 10 μm droplet is short compared with the timescales of the spray, namely the injection duration and the time-of-flight of the spray past a given axial station, so that this size can respond fairly well to the variations in the instantaneous velocity of the air. Even if this were not so, and the argument based on Stokes number suggests that it is, the comparisons between the behaviour of the different droplet sizes is of sufficient interest to justify the presentation of the results and discussion. In contrast, the relaxation times of 60 μm dia or larger droplets exceed the timescales of the spray, so that this size class retains the velocity at its formation for the duration of the abscissa of figure 2.

At the leading edge of the spray, measurable only at $z/D = 550$ and 780 (figure 2), the ensemble-averaged axial velocity of the 30 and 60 μm droplets is largest early in the spray, giving rise to rapid penetration, and decreases monotonically in the so-called "trailing edge" of the spray, defined as the region where $\partial U/\partial t$ is negative (Pitcher & Wigley 1989). The velocity at any instant increases with droplet size and this is true of all measured profiles. The shape of the temporal profile is partly the result of the injection schedule and partly the result of breakup, as is discussed below in section 4. A consequence of the schedule is that the time-of-flight of the cloud through the measurement volume increases from $\sim$3 to $\sim$4 times the injection duration at $z/D = 110$ and 780, respectively. As expected, the velocity of the air is close to zero as the leading edge of the spray arrives and then, within the spray body, increases to a maximum value as axial momentum is transferred from the droplets to the gas.

At $z/D = 110$, 220 and 440, results after the passage of the leading edge show that the axial velocity of all the droplets decreased monotonically with time. The absence at $z/D = 780$ of any velocities comparable with those at injection suggests that atomization after the beginning of

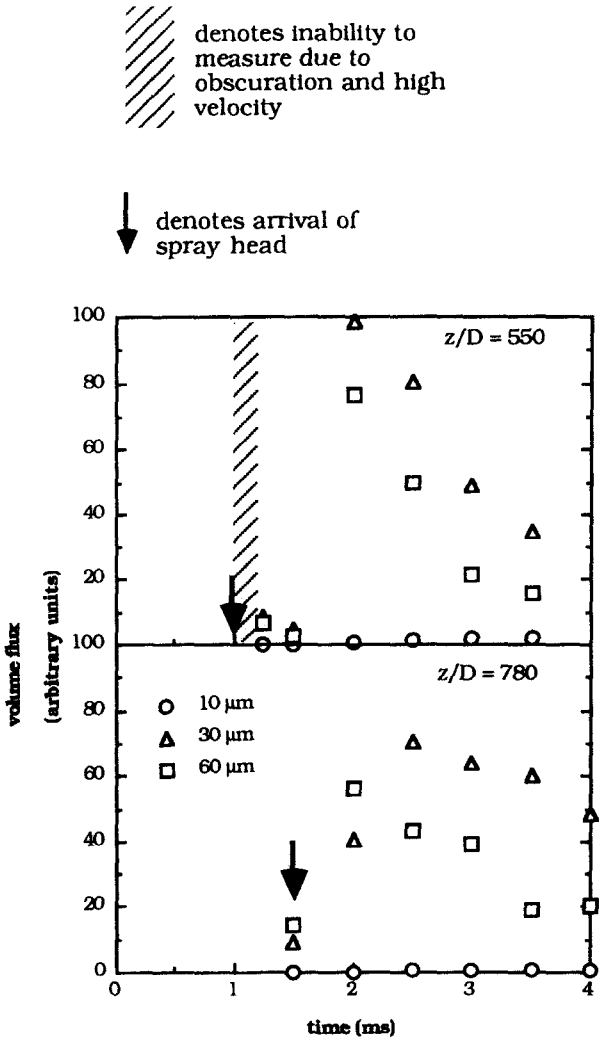

Figure 4. Temporal profiles of centreline volume flux at $z/D = 550$ and 780 carried by 10, 30 and 60 μm droplets.

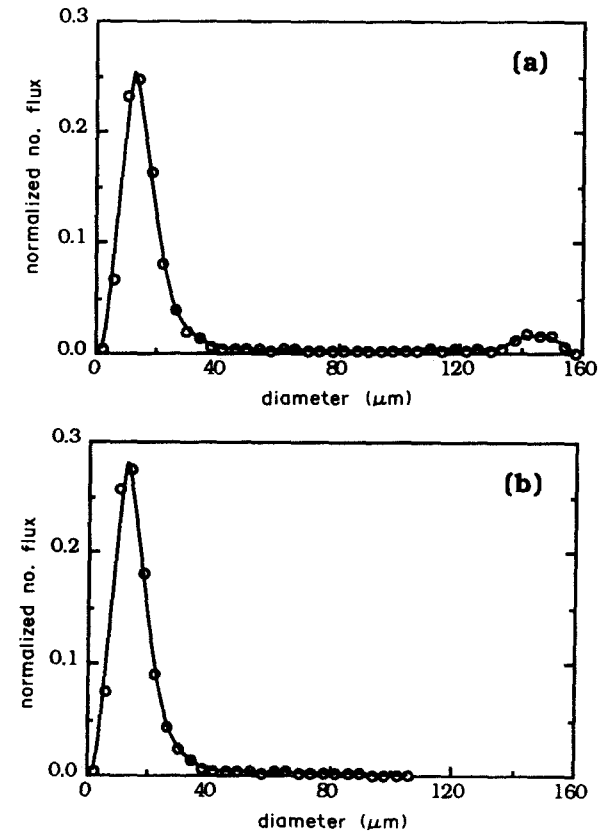

Figure 5. Droplet number flux distribution on centreline at $z/D = 110$ and 2.0 ms after the beginning of injection: (a) measured distribution; (b) corrected by truncation of the distribution beyond the minimum value occurring between 90 and 110 μm.

injection forms a large number of droplets with sufficiently small inertia to decelerate to velocities $<0.3\ U_0$ during the time of flight to $z/D = 780$, or in about 2 ms. This, in turn, implies that the relaxation times of the droplets correspond to a diameter of about 20 μm.

Figure 3 presents the RMS of the axial and radial velocity fluctuations, u' and v', at $z/D = 550$, which is sufficiently far downstream so that air has been entrained into the spray and some interaction between the two phases might be expected. The RMS of the axial velocity fluctuations for all three droplet sizes are large on arrival of the spray [figure 3(a)] and larger than the corresponding radial RMS velocity at the same location. This anisotropy is evidence that the axial RMS droplet velocity is acquired from three processes other than acquisition from the gaseous phase, as discussed below. As the cloud passes, the RMS of the axial velocity fluctuations decreases for all sizes but the RMS of the radial velocity fluctuations of the 10 μm droplets at $z/D = 550$ [figure 3(b)] increases, in contrast to those of the larger droplets which remain constant with time. Because the 10 μm droplets respond to the turbulence of the entrained air, they disperse away from the centreline.

3.1.2. Flux and mean diameters. The temporal variation of the volume flux, G_i ($m^3/m^2 \cdot s$), of the 10, 30 and 60 μm droplets on the centreline is shown in figure 4 for $z/D = 550$ and 780, with an ordinate in arbitrary units because approx. 75% of Doppler signals were discarded as a consequence of beam extinction. The *relative* flux of each droplet diameter is likely to be correct because measurements of the mean cross-sectional areas of the measuring volume for the given size classes (Saffman 1987; Hardalupas & Taylor 1989) show that it is virtually constant throughout the measurement period, particularly away from the centreline, at $z/D = 550$ and 780. This implies that any bias against, for example, the 10 μm class may be small. It should be noted that the measurement of SMD and AMD, as presented below and by other workers, necessarily implies the measurement of flux or, equivalently, number density. However a relative, rather than absolute, measurement is sufficient for the purpose of establishing the mean diameters. The uncertainty in the measurement of flux remains and is unlikely to be resolved completely until there has been further examination of the experimental technique.

The flux of the 60 μm droplets at the leading edge of the spray at $z/D = 780$ is initially larger than that of the 30 μm droplets and similar behaviour was observed at $z/D = 110$, but not at other stations. Hence the flux in the spray leading edge, at $z/D = 110$ and 780, is carried at first by 60 μm droplets and subsequently by slower moving 30 μm droplets. This observation is in contrast to the suggestion of Arcoumanis *et al.* (1990b), based on locations close to the nozzle and short times after injection, and it may be that their lower-velocity fine spray at the spray leading edge has been overtaken by the denser core at our measurement stations. In the trailing edge of the spray, the 30 μm droplets carry about twice the droplet flux of the 60 μm droplets. As expected, the proportion of flux in the 10 μm class is negligibly small.

The measured size distribution at 110 diameters from the nozzle, figure 5(a), shows a small isolated peak at around 140 μm which has a large influence on the local values of, for example, the SMD and volume flux. Similar peaks were found at the other locations and decrease with distance from the nozzle and later in time after the spray tip arrival. The peak occurs at diameters which are comparable with the nozzle exit diameter and Koo & Martin (1990) have measured 300 μm droplets produced by a 406 μm diesel injector, but without comment. In our measurements, the velocities associated with the peak suggest that these droplets will be far from spherical, because the likely relative velocities and associated Weber and Ohnesorge numbers, discussed in the appendix, exceed the critical values which lead to breakup. Alexander *et al.* (1985) have shown that a phase-Doppler anemometer can overestimate the size of ellipsoids with aspect ratios around 0.7 by as much as 45%, so that diameters above about 100 μm could be regarded as a qualitative indication of the presence of large droplets. An alternative plausible explanation for the isolated peak might be a poor signal-to-noise ratio or multiple occupancy of the measuring volume. Whatever the origin of the peak, it appears wise to truncate the distribution so as to exclude the peak.

The mean diameters were calculated from size distributions excluding the non-spherical droplets, which were removed by discarding readings above the minimum value of the number flux occurring between 90 and 110 μm. An example of the truncated distribution is shown in figure 5(b) and numerical experiments showed that the resulting tolerance on the SMD was around 10%.

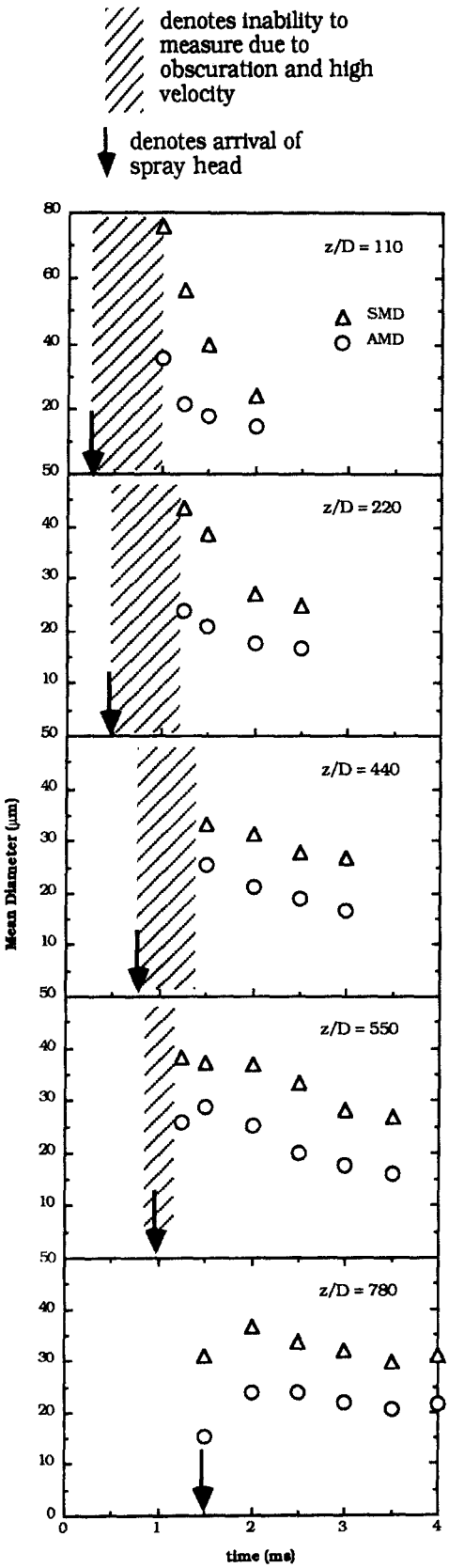

Figure 6. Temporal profiles of the centreline SMD and AMD at $z/D = 110$, 220, 440, 550 and 780 for 10, 30 and 60 μm droplets.

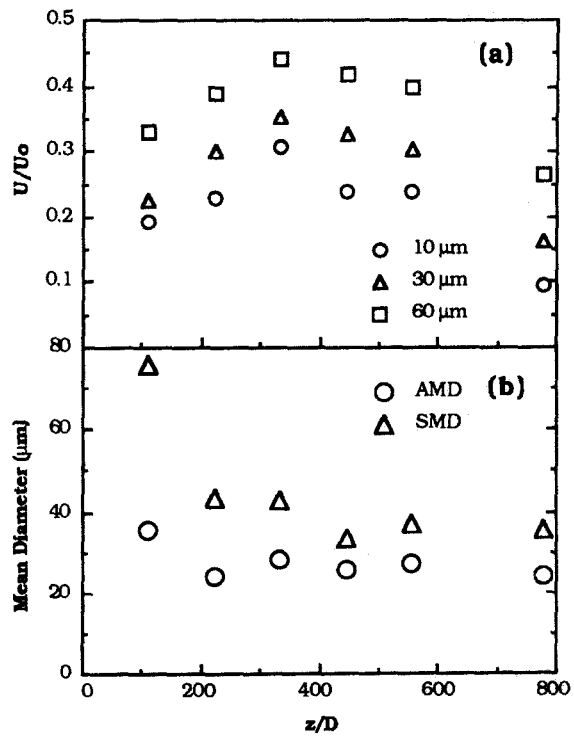

Figure 7. Centreline development at 0.7 ms after arrival of the spray tip at the measurement location of: (a) the ensemble-averaged axial velocity of 10, 30 and 60 μm droplets; (b) SMD and AMD.

At $z/D = 550$ and 780, the maximum SMD and AMD on the centreline are, respectively, between about 38 and 28 μm and occur at about 1.5 and 2 ms after injection has started, figure 6. The beginning of the spray cloud consists of finer droplets than those after about 0.5 ms of transit by the cloud. The AMD and SMD decrease by up to about 10 μm after the occurrence of the maximum because smaller droplets, which lose their momentum rapidly, have been overtaken by the larger, faster droplets. It should be noted that the last measured point in each temporal profile of figure 6 represents the point at which there is no longer a large difference between the velocities of each size class, rather than the end of the spray. This arises where the entrained air has come into equilibrium with the particulate phase.

The mean diameters are larger at stations closer to the nozzle and this implies a reduction in diameter downstream of $z/D = 110$. At $z/D = 440$, for example, the maximum SMD and AMD are between 30–40 and 20–30 μm, respectively, and the former agree well with results of Sato (1985) and Shimizu & Emori (1987). Closer to the nozzle, $110 < z/D < 220$, the maximum SMD is between 50–80 μm, similar to the measurements of Koo & Martin (1990), although extrapolation suggests that higher values exist during the unmeasurable part.

SMD values obtained from Fraunhofer diffraction in the same spray (Arcoumanis *et al.* 1990a) decreased during the temporal profile at $z/D = 110$ by $< \sim 15$ μm, in constrast to about 60 μm in figure 6. The difference is due to the average formed by the Fraunhofer diffraction instrument, as quantified, for example, by Cossali & Hardalupas (1992), and to *local* extinction of the incident laser beam in excess of 50% which, as shown by the work of Dodge (1984), lead to underestimation of the mean diameter. The larger increase in the SMD, as compared with the AMD, as the nozzle is approached suggests that larger droplets dominate in the main spray region because the SMD is affected more by the larger droplets than is AMD (Tate 1982). The observation could also be due to the presence of ligaments and non-spherical droplets which are known to exist in large number up to around $z/D = 50$ (Cavaliere *et al.* 1988) and possibly up to $z/D = 150$ (Yule *et al.* 1985). Further support for this conclusion is provided by the velocity measurements which, as discussed below, suggest spherical droplets will not be stable.

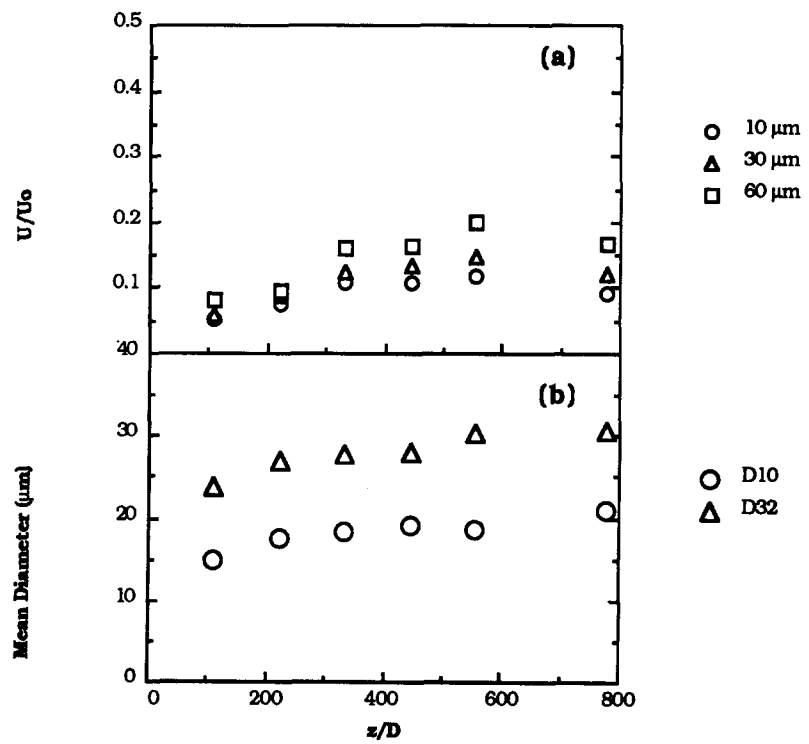

Figure 8. Centreline development at 1.8 ms after arrival of the spray tip at the measurement location of: (a) ensemble-averaged axial velocity of 10, 30 and 60 μm droplets; (b) SMD and AMD.

3.2. Spatial centreline characteristics

Figures 7 and 8 show spatial centreline profiles of velocity and mean diameter at 0.7 and 1.8 ms after the arrival of the spray tip, respectively, obtained by interpolation of the temporal profiles of the preceding section. The chosen times correspond to the earliest and latest times for which complete spatial information exists. The spray tip arrival time at a given location close to the nozzle is taken from Arcoumanis *et al.* (1990a) and the measurements were extended here to locations far downstream of the nozzle (table 3), using the time at which the first Doppler signal occurred. Figures 7(a) and 8(a) show that the ensemble-averaged axial velocities of the 10, 30 and 60 μm

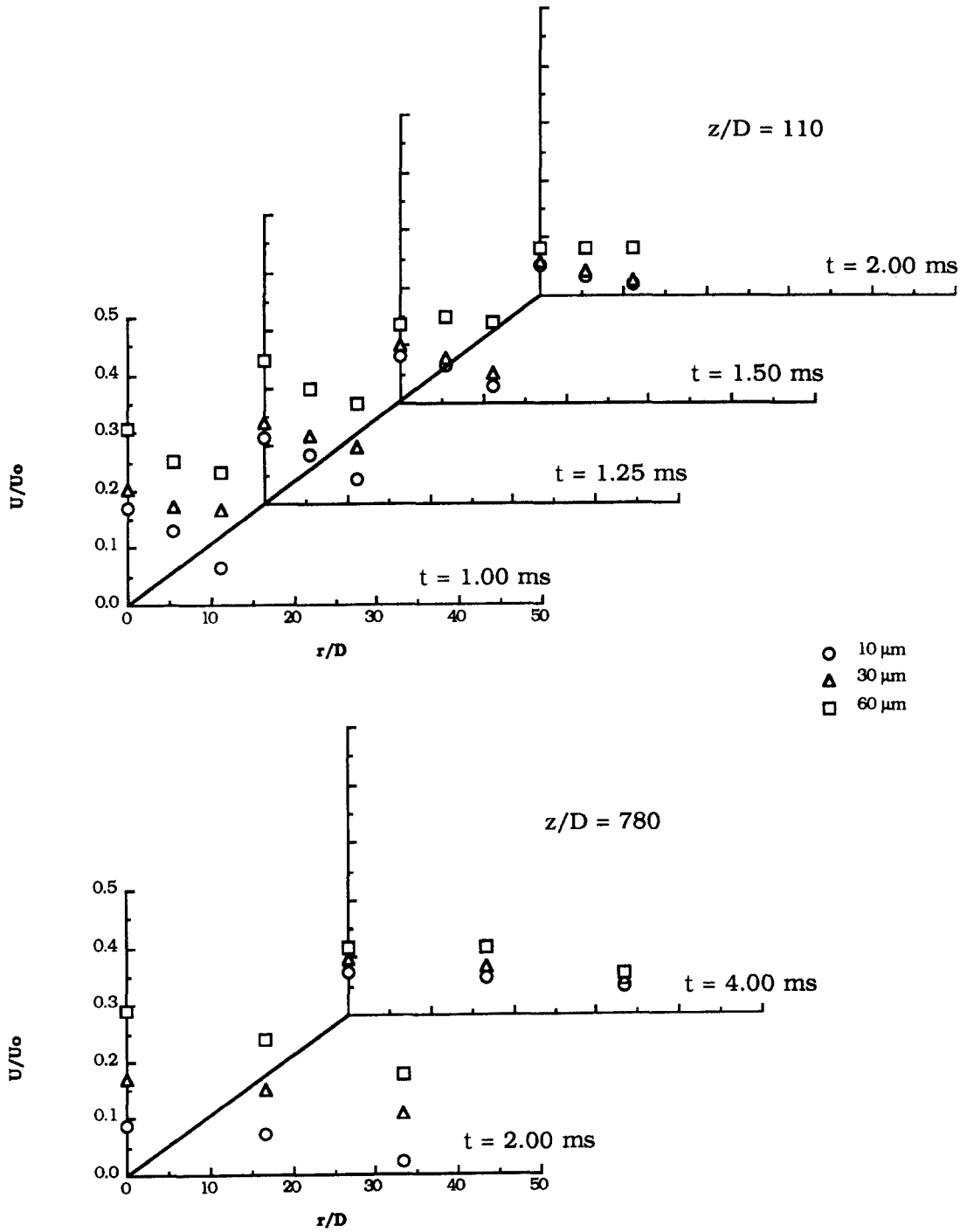

Figure 9. Radial profiles of ensemble-averaged axial velocity of 10, 30 and 60 μm droplets at $z/D = 110$ and 780 at different times after the beginning of injection.

droplets reach maximum values at $z/D \approx 300$ and 600, respectively. The increase in velocity along the centreline implies that the cloud becomes longer as it travels downstream and confirms that "late, fast" droplets, which are produced later in the injection, overtake the "early, slow" droplets. The late droplets are faster than the early droplets due to the injection schedule and this is reinforced by the reduced air drag experienced by droplets generated later in the injection process because the air has already been set in motion.

Figure 8(b) shows that the mean diameters decrease rapidly over the first 200 diameters from the nozzle and is the spatial counterpart of the trend observed in the temporal profile in figure 6. In contrast, figure 8(b) shows that 1.8 ms after tip arrival the mean diameters in the cloud *increase*. This is probably due to the larger droplets retaining their velocity for longer times due to the longer relaxation times [table 2(a)], as demonstrated in figure 2, thereby changing the relative concentration of smaller droplets at a given temporal location in the cloud. This effect acts to increase the relative concentration of the larger diameters, as the smaller droplets remain either farther behind in the spray or disperse from the centreline.

3.3. Radial profiles

The spread of the spray is quantified by the radial profiles of U, u', G_i, d_{32} and d_{10} and selected measurements are presented in figures 9–12, respectively. The spray was symmetrical and its growth was characterized by the half-width of the ensemble-averaged velocity of the 10 μm class, which was measured to a tolerance of $\pm 20\%$, to be 8, 13, 27 and 30 mm at $z/D = 110$, 220, 440 and 780, respectively.

Figure 9 shows that the maximum axial velocities occur on the axis, at $z/D = 110$ and 780, and that the larger droplets move consistently faster than the smaller droplets everywhere. The magnitudes of the relative velocities between the 60 μm droplets and the air decrease with time after injection: the maximum values in figure 9 are of the order of 0.15 and 0.2 U/U_0 for $z/D = 110$ and 780, respectively. The largest relative velocity was 0.3 U/U_0 which occurred at $z/D = 550$ at 1.25 ms after injection, in results not presented here. The evidence suggests that the relative velocity is, for $z/D = 110$ and at the times measured, almost as large near the edge of the spray as near the centreline. Farther downstream, the magnitude of the relative velocity at the edge of the spray tends to become smaller than near the axis.

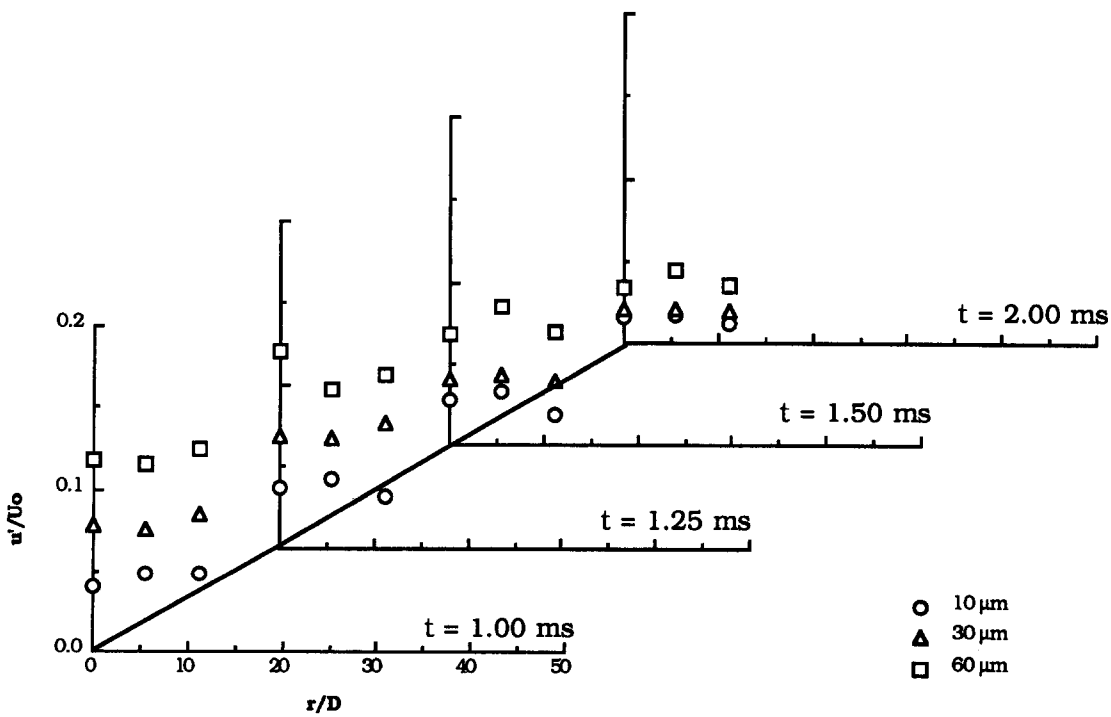

Figure 10. Radial profiles of axial RMS velocity of 10, 30 and 60 μm droplets at $z/D = 110$ at different times after the beginning of injection.

The corresponding values of u'/U_0, figure 10, quantify the net effects of the air turbulence, the repeatability of the injection process and fluctuations due to fan spreading and overtaking, as explained in section 3.1. In general, the fluctuations are almost constant across each profile and decrease with time after injection. Close to the injector, e.g. at $z/D = 110$, the fluctuation levels

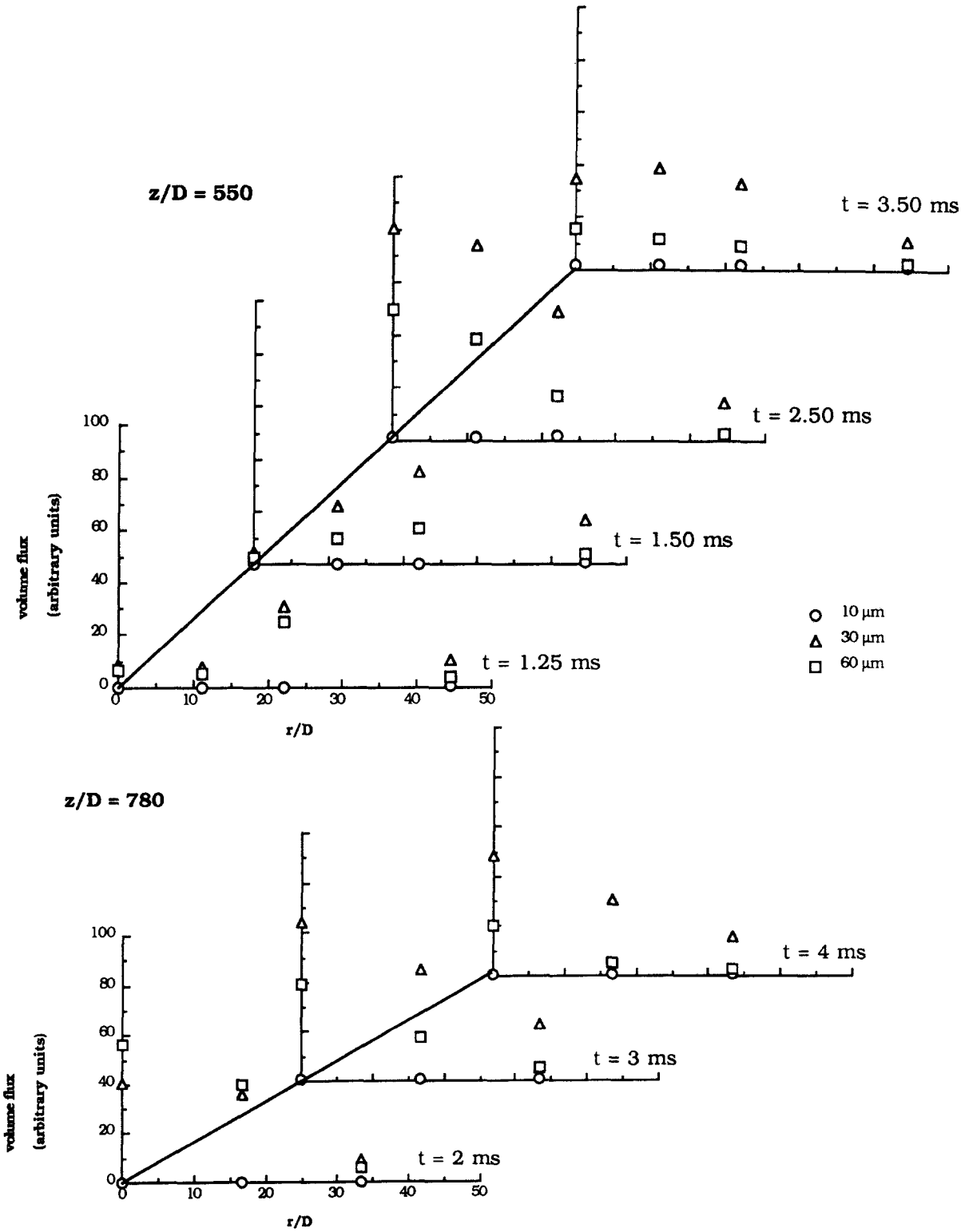

Figure 11. Radial profiles of volume flux carried by the 10, 30 and 60 μm droplets at $z/D = 550$ and 780 at different times after the beginning of injection.

increase with diameter, with the largest measured value being about $0.12\,U_0$. With increasing distance from the injector, e.g. at $z/D = 780$ and not shown here, the RMS velocity of the 10 μm droplets, and hence by implication of the air, is similar to the fluctuations of the droplet for both size classes, indicating that the gaseous phase is more turbulent than it was close to the injector. It is likely that, given the high volume fraction of liquid and the time constant associated with 30 and 60 μm droplets, the air turbulence is increased by the droplets, rather than the droplets' RMS velocity being increased by acquiring turbulence from the air.

The high axial RMS velocity fluctuations of the droplets are mainly the result of three mechanisms. The first is the fan-spreading effect identified by Hardalupas *et al.* (1989) in which the RMS droplet radial velocity and the radial profile of ensemble-averaged droplet axial velocity, e.g. as in figure 2, combine to produce high values of RMS droplet axial velocity. The second mechanism is provided by the transient nature of the spray. Droplets of a given size produced at the beginning of injection will have smaller velocities than those produced later as a direct consequence of the injection schedule. Velocity measurements of this given droplet size, made downstream of the point at which the droplets were first formed, will include signals from the "late-injected, fast" droplets overtaking the "early-injected, slow" droplets. This has the effect of producing large droplet axial RMS velocities. Both of these mechanisms give rise to axial droplet RMS velocities without reference to transfer from the turbulence of the gaseous phase. The third mechanism is the tolerance on the repeatability of the injection process.

Figure 11 shows the radial profile of the volume flux, G_i, of the 10, 30 and 60 μm droplets at $z/D = 550$ and 780 as a function of time after injection. Once again, the effects of extinction are such that it is the flux of each size class relative to the other two at each point that should be considered. For example, the minimum in the flux of the 30 and 60 μm droplets, shown in figure 11, for $z/D = 550$ and at $t = 1.25$ ms may be the effect of the reduced data rate at the centreline due to extinction. Pitcher & Wigley (1989) have interpreted similar shapes of profiles of droplet concentration as support for the notion that aerodynamic forces generate better atomization on the spray periphery than on the centreline. While this interpretation is consistent with their photographic evidence, it remains possible that the result is an artifact of the extinction. The figure does show, however, that the flux of the liquid carried by the 30 μm droplets is larger than that of the 60 μm droplets across the whole profile, even though the latter move faster. The 30 μm droplets carry the larger flux because their concentration is higher, as reflected by the value of the SMD.

Figure 12 shows that the edge of the spray is more finely atomized than is the centre so that the SMD and AMD fall from the centreline value by up to 30 and 25 μm, respectively, at $z/D = 110$ and $t = 1.0$ ms. This may be due to small, say 10 μm, droplets responding to the air motion and dispersing radially faster than the larger droplets. The alternative hypothesis is that the atomization at the edge of the spray is more efficient than near the centre (e.g. Pitcher & Wigley 1989) and, although intuitively appealing, is not demonstrably true because the magnitude of the relative velocity is no larger at the edge than at the centre, at least in the measurable part of the spray development. The width of the size distribution, quantified by the difference between the SMD and AMD, decreases at the edge of the spray, with distance from the injector and towards the end of injection. Thus, for example, the maximum measured SMD and AMD are of the order of 80 and 40 μm on the centreline at $z/D = 110$ and 1.0 ms after the beginning of injection but have fallen to <30 and <20 μm, respectively, at the same location by 2.0 ms after injection. However, by $z/D = 780$, where the whole spray can be measured, the radial and temporal variations in both SMD and AMD are only of the order of 10 and 5 μm, respectively.

4. DISCUSSION

The measurements presented in the preceding section show that the spray became finer with increasing distance from the injector. For example, between $z/D \approx 100$ and ≈ 780, the centreline SMD decreases from a maximum measured value of around 80 to about 38 μm. The question arises as to whether this reduction in SMD is due to the breakup of droplets as a result of the magnitude of the relative velocity between the droplets and the air. Pilch & Erdman (1987) have suggested that the critical Weber number for breakup is 12, based on the relative velocity, ΔU_s. Figure 13 quantifies the corresponding critical relative velocities for the 60 and 30 μm droplets as

$\Delta U_s/U_0 = 0.53$ and 0.76, respectively, and the details of the calculation are given in the appendix. The magnitude of the air velocity, which is needed for estimation of ΔU_s can be closely approximated by the velocity of the 10 μm droplets. For $z/D < 550$, extrapolation of the measured velocities of figure 2 into the unmeasurable region suggests that the velocity of the droplets at the leading edge of the spray will result in relative velocities which are likely to exceed the critical values and give rise to extensive breakup. This is partly confirmed at $z/D = 550$, taken immediately after the arrival of the leading edge of the spray, at $t = 1.25$ ms when the relatives velocity of the 60 μm droplets is $\Delta U_s/U_0 \approx 0.35$. Backward extrapolation to the leading edge, 0.25 ms earlier when the velocity of the air is zero, suggests that the value of $\Delta U_s/U_0$ is about 0.45 U_0, and hence close to the critical value quoted above.

The maximum magnitude of the ensemble-averaged relative velocities for the 60 μm droplets of figures 3, 8 and 9 is, with the exception given as the end of the preceding paragraph, only about

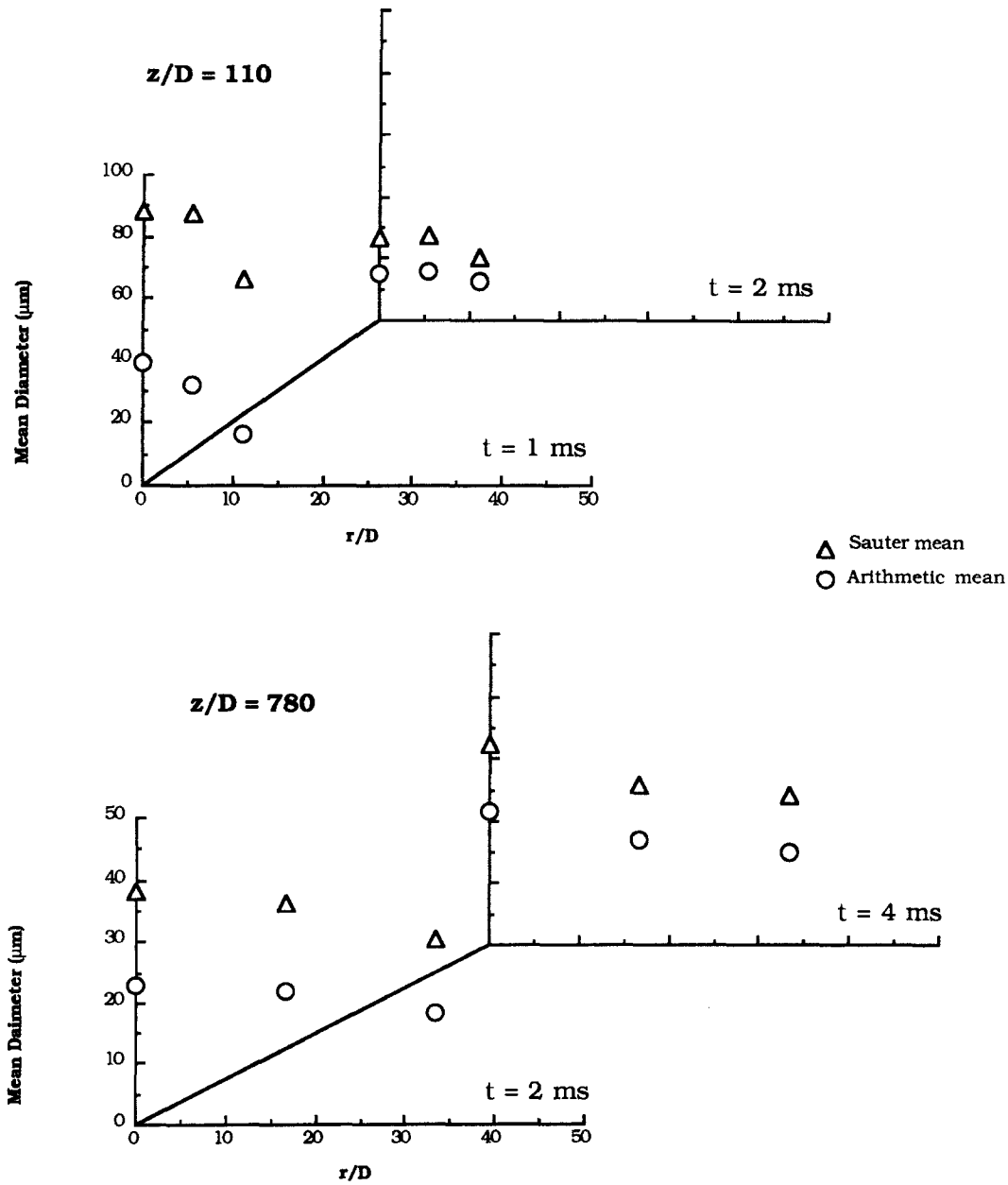

Figure 12. Radial profiles of SMD and AMD at $z/D = 110$ and 780 at different times after the beginning of injection.

40% of the required critical values. The measurements quoted in the opening sentences of the preceding paragraph show that the SMD decreases during the measurable part of the spray. Arguments to justify breakup might rest on either uncertainties in Pilch & Erdman's (1987) value of the critical Weber number or on the magnitude of the *instantaneous* relative velocity being larger than the ensemble-averaged value, but neither is convincing. In the former case, even an uncertainty of a factor of 2 is not enough to justify breakup. For the latter, an estimate of the peak instantaneous value of $\Delta U_s/U_0$ can be made as $(U_d + u'_d) - (U_a - u'_a)$, where subscripts d and a refer to the diesel droplets of diameter d and air phase velocities and U and u' refer to the measured ensemble-averaged and RMS velocities, respectively. The measurements of figures 3 and 10 suggest that $u' \approx 0.1\ U$ for both phases and the resulting estimate of the peak value of the relative velocity is insufficient to give rise to breakup. Another potential argument for a large instantaneous relative velocity might be based on the fan-spreading effect of Hardalupas *et al.* (1989), whereby fluctuations of droplet radial velocity v'_d, e.g. as in figure 3(b), transport droplets off the centreline and into regions of lower ensemble-averaged air velocity, as the measurements of figure 9 indicate. The instantaneous value of $\Delta U_s/U_0$ can be estimated as $(U_{d,c} - U_{a,r})$. The subscript d, c refers to the ensemble-averaged centreline diesel velocities and a, r to the ensemble-averaged air velocity, at a radius from the centreline of r, evaluated downstream of the axial station at which $U_{d,c}$ is found. Once again, the magnitude of $(U_{d,c} - U_{a,r})$ is too small to provide convincing justification for breakup due to slip.

The SMD of the spray downstream of the leading edge reduces up to a distance of about $z/D = 400$, as shown, for example, by the results of figure 7, for the particular case of 0.7 ms after the tip arrival. *In this part of the spray*, in other words away from the leading edge, the most likely explanation for the reduction is that it is due to the appearance of small droplets in the size distribution, rather than to the destruction of the large diameters through breakup. The source of the small droplets is the breakup of the spray at the leading edge, the unmeasurable part of the spray, corresponding—at most—to the first 0.5 ms in the passage of the spray. There, the required large relative velocities exist to produce Weber numbers in excess of the critical value and, for example, this mechanism is the source of the observed low-speed 10 μm droplets at $z/D = 550$ in figure 2 at $t \approx 1.25$ ms. The breakup at the leading edge also contributes to the reduction in drop diameter *at* the leading edge with increasing downstream distance. An important difference between a steady and an unsteady spray, from the point of view of atomization, is that larger relative velocities can be generated at the leading edge of the unsteady spray than can be sustained in a steady spray, and this difference leads to more efficient atomization in the unsteady spray.

Once generated at the leading edge, the small droplets lose velocity due to drag from the surrounding slower-moving air and, given that table 3 implies that the spray tip velocity is constant at about 0.75 U_0, hence these get left behind to form the slower, measurable part of the spray. The evidence of figure 2, and of the profile at $z/D = 550$ in particular, shows that *most of* the generation is restricted to transit of less than the first 0.5 ms of the spray leading edge and, given the tip speed of about 100 m/s $\approx 0.75\ U_0$ from table 3, corresponds to no more than the first 50 mm

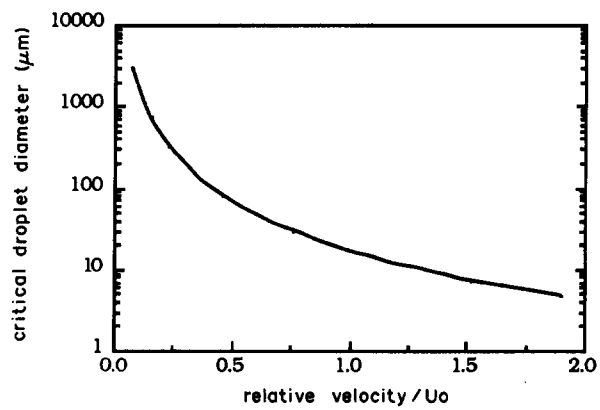

Figure 13. Variation of critical droplet diameter for breakup (We = 12) as a function of the droplet relative velocity.

of the spray. An explanation of the origin of the 10 μm droplets, measured at distances beyond $z/D = 550$, is that these are convected from upstream stations *together* with the leading edge, given that the entrained air and, at least, the 30 μm droplets move at almost the same mean velocity. The low volume flux of the 10 μm droplets, relative to the other sizes as shown in figure 4, is consistent with this description. It would be of some interest to investigate this question further.

In the absence of direct evidence for the atomization at the leading edge, one way to substantiate the preceding explanation is to demonstrate that it is consistent with the time intervals and length scales available. The first process is generation of the small droplets: the associated breakup timescale is shown, in the appendix, to be so small in relation to the other timescales that it is effectively instantaneous. The second process is the small droplet deceleration from the high velocity associated with the "parent" large droplet at the leading edge. If atomization results mostly in diameters of between 10 and 20 μm, as suggested by the value of the SMD and by the relative magnitude of the fluxes in figures 11 and 12, deceleration to the velocity of the surrounding air will occur over times comparable with the relaxation times given in table 2, namely between 1/4 and 2 ms. During these times, the droplets will have travelled distances of between about 70 and 590D, assuming that average droplet velocities are of the order of 0.4 U_0, corresponding to the measured velocity of the faster droplets. These distances are comparable to that over which the SMD reduces and imply that the relaxation to the air velocity can occur in the available length scales. The above arguments suggest that break up ceases by about $z/D = 550$, where coincidentally measurements are no longer subject to uncertainty due to high velocities or large extinction.

The results of this paper are interesting as part of the spectrum of results which can be obtained at pressures between atmospheric and those typical of a diesel engine at the beginning of injection, say 50 bar and 1000 K. Although other parameters are also relevant to the classification of the flow and the atomization, our discussion has been conducted in terms of Weber numbers. This allows us to extend the generality of our results, at least qualitatively, to conditions more representative of those in engines. The Weber number will be affected by the decrease in the surface tension of the liquid and the increase in the air density, say by factors of 1/2 and 20 respectively. The spray velocity, and hence also the magnitude of the relative velocity, will be lower at high pressure (e.g. Yule & Aval 1989) by a factor of perhaps 1/2, so that the net effect on the Weber number will be to change it from the conditions of this paper by an overall factor of about an order of magnitude. As a consequence, and as might be expected, a larger fraction of the spray will have a Weber number larger than the critical value for breakup and hence atomization will be complete in shorter distances from the nozzle than in this work.

5. CONCLUSIONS

The Bosch diesel injector was operated unsteadily in the ambient atmosphere, at a frequency corresponding to 1200 rpm of a four-stroke engine. The main conclusions are as follows:

(a) The spray became finer with increasing distance from the injector and tended to be better atomized on the periphery, i.e. away from the centreline and at the leading and trailing edges. Near to the injector, at $z/D \approx 100$, the centreline SMD decreases from a maximum measured value of around 80 μm at $t = 1.0$ ms to about 28 μm at $t = 2.0$ ms; the corresponding values at the spray edge are about 60 and 20 μm, respectively. The decrease is due to processes described in points (c) and (d) below. Far from the injector, at $z/D \approx 780$, the centreline maximum and minimum values have fallen to about 38 and 30 μm at $t = 2.0$ and 4.0 ms, respectively; the corresponding values at the spray edge are about 30 and 25 μm.

(b) Far from the injector, at $z/D > 550$, the diesel flux carried by the 30 μm droplets is generally about twice as large as that carried by the 60 μm droplets, although larger droplets move faster than the smaller droplets.

(c) Droplet breakup is caused by the magnitude of the relative velocity, ΔU_s, resulting in Weber numbers exceeding a critical value. Sufficiently larger relative velocities may have occurred during the first 0.5 ms interval after the arrival of the first droplets, corresponding to the unmeasurable part of the leading edge of the spray, up to $z/D \approx 550$.

(d) The reduction in the SMD in the measurable part occurs through the progressive accumulation of droplets with diameters $<20\,\mu$m which are generated in the unmeasurable part and, due to drag from the surrounding air, are left behind by the fast-moving leading edge of the spray to form the slower, measurable part of the spray. With the exception of the leading edge at $z/D = 550$, breakup does not occur within the measurable part of the spray because the values of the Weber number, associated with the observed values of ΔU_s, are below the critical value for all measured diameters. The value of ΔU_s decreases with decreasing droplet diameter, because of the lower relaxation times. The large RMS axial velocity of the larger droplets is due to the "overtaking" and fan-spreading effects and not to their response to the entrained air turbulence.

An important difference between a steady and an unsteady spray, from the point of view of atomization, is that larger relative velocities can be generated at the leading edge of the unsteady spray than can be sustained in a steady spray, and this difference leads to more efficient atomization in the unsteady spray.

(e) During spray movement away from the nozzle, larger droplets tend to concentrate at the leading edge because the smaller droplets lose momentum faster and hence are overtaken. The spray elongates as it travels downstream because of the shape of the injection schedule and also because of the difference in the relaxation times of the various droplet sizes in the spray.

Acknowledgements—The Ford Motor Company Ltd and the Commission of the European Community have provided support for the experiment. The authors would like to thank Drs C. Arcoumanis and E. Cossali for their help during the experiment. Mr J. R. Laker designed the phase-Doppler counter. A.M.K.P.T. was supported by a 1983 Royal Society University Research Fellowship.

REFERENCES

ALEXANDER, D. R., WILES, K. J., SCHAUB, S. A. & SEEMAN, M. P. 1985 Effects of non-spherical drops on a phase Doppler spray analyser. In *Particle Sizing and Spray Analysis* (Edited by CHIGIER, N. & STEWART, G. W.). *Proc. SPIE* **573**, 67–72.

ANON. 1971 Fuel injection equipment for diesel engines: fuel injection pumps PE and PF. In *Bosch Technical Instruction Series*, Publ. VDT-UBP 001/15 B (Edited by ADLER, U. & KAUFMANN, E.). Robert Bosch GmbH, Abt. KH/VDT, Stuttgart.

ARAI, M., SHIMIZU, M. & HIROYASU, H. 1985 Breakup length and spray length angle of high speed jet. In *Proc. 3rd Int. Conf. on Liquid Atomisation and Spray Systems (ICLASS)*, London, Paper IB/4/1.

ARCOUMANIS, C., COSSALI, E., PAAL, G. & WHITELAW, J. H. 1990a Transient characteristics of multi-hole diesel sprays. Presented at the *Int. Congr. and Exposition*, Detroit, MI, SAE Paper 900480.

ARCOUMANIS, C., PAAL, G. & WHITELAW, J. H. 1990b Application of laser techniques to diesel engine sprays. Presented at the *5th Int. Symp. on the Applications of Laser Techniques to Fluid Mechanics*, Lisbon, Portugal, Paper 14.5.

BACHALO, W. D., HOUSER, M. J. & SMITH, J. N. 1986 Evolutionary behavior of sprays produced by pressure atomisers. Paper AIAA-86-0296.

CAVALIERE, A., RAGUCCI, R., D'ALESSIO, A. & NOVIELLO, C. 1988 Analysis of diesel sprays through two-dimensional laser light scattering. In *Proc. 22nd Symp. (Int.) on Combustion*, The Combustion Institute. pp. 1973–1981.

COSSALI, E. & HARDALUPAS, Y. 1992 Comparison between laser diffraction and phase Doppler velocimeter techniques in dense, small width sprays. *Expts Fluids*. In press.

DODGE, L. G. 1984 Change of calibration of diffraction-based particle sizers in dense sprays. *Opt. Engng* **23**, 626–630.

FELTON, P. G., MANTZARAS, J., BARDSLEY, M. E. A. & BRACCO, F. V. 1987 2-D visualisation of liquid fuel injection in an internal combustion engine. Paper SAE 872074.

FUCHS, N. A. 1964 *The Mechanics of Aerosol*. Pergamon Press, Oxford.

HARDALUPAS, Y. 1989 Experiments with isothermal two-phase flows. Ph.D. Thesis, Univ. of London.

HARDALUPAS, Y. & TAYLOR, A. M. K. P. 1989 On the measurement of particle concentration near a stagnation point. *Expts Fluids* **8**, 113–118. See also, Erratum. *Expts Fluids* **9**, 356.

HARDALUPAS, Y., TAYLOR, A. M. K. P. & WHITELAW, J. H. 1988 Depth of field considerations in particle sizing using the phase-Doppler technique. In *Laser Anemometry in Fluid Mechanics* (Edited by ADRIAN, R. J., ASANUMA, T., DURAO, D. F. G., DURST, F. & WHITELAW, J. H.), pp. 347–360. LADOAN—Instituto Superior Tecnico, Lisbon, Portugal.

HARDALUPAS, Y., TAYLOR, A. M. K. P. & WHITELAW, J. H. 1989 Velocity and particle flux characteristics of turbulent particle-laden jets. *Proc. R. Soc. Lond.* **A426**, 31–78.

HARDALUPAS, Y., TAYLOR, A. M. K. P. & WHITELAW, J. H. 1990a Velocity and size characteristics of liquid-fuelled flames stabilised by a swirl burner. *Proc. R. Soc. Lond.* **A428**, 129–155.

HARDALUPAS, Y., TAYLOR, A. M. K. P. & WHITELAW, J. H. 1990b Unsteady sprays by a pintle injector. *JSME Int. J. Ser. II* **33**, 177–185.

HARDALUPAS, Y., TAYLOR, A. M. K. P. & WHITELAW, J. H. 1990c Fringe count limitations on the accuracy of the velocity and mass flux measurements in two-phase flows. Presented at the *5th Int. Symp. on the Applications of Laser Techniques to Fluid Mechanics*, Lisbon, Portugal, Paper 11.6.

KLIAFAS, Y., TAYLOR, A. M. K. P. & WHITELAW, J. H. 1985 Errors in particle sizing by LDA due to turbidity in the incident laser beams. *Expts Fluids* **5**, 159–176.

KLIAFAS, Y., TAYLOR, A. M. K. P. & WHITELAW, J. H. 1990 Errors due to turbidity in particle sizing using laser-Doppler anemometry. *Trans. ASME Jl Fluids Engng* **112**, 142–148.

KOO, J-Y. & MARTIN, J. K. 1990 Droplet sizes and velocities in a transient diesel fuel spray. Paper SAE 900397.

MAEDA, M., HISHIDA, K., SEKINE, M. & WATANABE, N. 1988 Measurements on spray jet using LDV system with particle size discrimination. In *Laser Anemometry in Fluid Mechanics* (Edited by ARIAN, R. J., ASANUMA, T., DURAO, D. F. G., DURST, F. & WHITELAW, J. H.), pp. 375–386. LADOAN—Instituto Superior Tecnico, Lisbon, Portugal.

NAKAYAMA, M. 1987 Development of a time-resolved particle sizer and spray sizing in high back-pressure injection. In *Laser Diagnostics and Modelling of Combustion* (Edited by IINUMA, K., ASANUMA, T., OHSAWA, T. & DOI, J.). Springer-Verlag, Berlin.

OBOKATA, T., INABA, K. & TAKAHASHI, H. 1988 LDA measurement of diesel spray and entrainment air flow. Presented at the *4th Int. Symp. on Applications of Laser Anemometry to Fluid Mechanics*, Lisbon, Portugal, Paper 3.15.

PILCH, M. & ERDMAN, C. A. 1987 Use of breakup time data and velocity history data to predict the maximum size of stable fragments for acceleration-induced breakup of a liquid drop. *Int. J. Multiphase Flow* **13**, 741–757.

PITCHER, G. & WIGLEY, G. 1989 Velocity and dropsize measurements in fuel sprays in a direct injection diesel engine. In *Proc. Int. Conf. on Mechanics of Two-phase Flows*, Taipei, Taiwan, pp. 291–298.

PITCHER, G., WIGLEY, G. & SAFFMAN, M. 1990 Sensitivity of dropsize measurements by phase Doppler anemometry to refractive index changes in combusting fuel sprays. Presented at the *5th Int. Symp. on Applications of Laser Techniques to Fluid Mechanics*, Lisbon, Portugal, Paper 14.4.

SAFFMAN, M. 1987 Automatic calibration of LDA measurement volume size. *Appl. Opt.* **26**, 2592–2597.

SAFFMAN, M., FRAIDL, G. K. & WIGLEY, G. 1988 Application of phase and laser Doppler anemometry to the measurement of droplet size and velocity in gasoline and diesel fuel injection

systems. Presented at the *4th Int. Symp. on Applications of Laser Anemometry to Fluid Mechanics*, Lisbon, Portugal Paper 5.15.

SATO, G. T. 1985 Structure of diesel spray. In *Proc. 3rd Int. Conf. on Liquid Atomisation and Spray Systems (ICLASS)*, London, Paper IP/1/1.

SHIMIZU, I. & EMORI, Y. 1987 Determination of the characteristics of diesel spray by the bidirectional light scattering image processing method. In *Laser Diagnostics and Modelling of Combustion* (Edited by INUMA, K., ASANUMA, T., OHSAWA, T. & DOI, J.). Springer-Verlag, Berlin.

TAMATA, M., ARAI, M. & HIROYASU, H. 1985 Effect of fuel viscosity and surface tension on diesel spray drops. In *Proc. 3rd Int. Conf. on Liquid Atomisation and Spray Systems (ICLASS)* London, Paper IIB/1/1.

TATE, R. W. 1982 Some problems associated with the accurate representation of droplet size distributions. In *Proc. 1st Int. Conf. on Liquid Atomisation and Spray Systems (ICLASS)*, Madison, WI.

WU, K. J., COGHE, A., SANTAVICCA, D. A. & BRACCO, F. V. 1984 LDV measurements of drop velocity in diesel-type sprays. *AIAA Jl* **22**, 1263–1270.

YULE, A. J. & AVAL, S. M. 1989 A technique for velocity measurement in diesel sprays. *Combust. Flame* **77**, 385–394.

YULE, A. J., MO, S. L., THAM, S. Y. & AVAL, S. M. 1985 Diesel spray structure. In *Proc. 3rd Int. Conf. on Liquid Atomisation and Spray Systems (ICLASS)*, London, Paper IIB/2/1.

APPENDIX

Calculation of Weber Numbers and Typical Breakup Times

There are three characteristic numbers which describe the breakup of an accelerated droplet:

$$\text{Weber number} \qquad \mathrm{We} = \frac{\rho \Delta U_s^2 d}{\sigma}, \qquad [A.1]$$

$$\text{Ohnesorge number} \qquad \mathrm{On} = \frac{\mu_d}{(\rho_d d\sigma)^{0.5}}, \qquad [A.2]$$

and

$$\text{Dimensionless time} \qquad T = t\Delta U_s \left(\frac{\rho}{\rho_d}\right)^{0.5} d^{-1}, \qquad [A.3]$$

where ρ is the density of the surrounding fluid, ρ_d is the density of the droplet, μ_d is the dynamic viscosity of the droplet, σ is the surface tension of the droplet, d is the droplet diameter, ΔU_s is the relative velocity between the droplet and the surrounding fluid and t is the dimensional time. The dimensionless time is the characteristic of droplet breakup of Rayleigh–Taylor instabilities.

Pilch & Erdman (1987) suggested that the non-dimensional time to initiate breakup, T_i, is given by

$$T_i = 1.9\,(\mathrm{We} - 12)^{-0.25}(1 + 2.2\,\mathrm{On}^{1.6}) \qquad [A.4]$$

and for low viscosity droplets, when On is very small (On < 0.1), the total breakup time is

$$T_i = 6\,(\mathrm{We} - 12)^{-0.25} \quad 12 < \mathrm{We} < 18. \qquad [A.5.]$$

Using the above relations, the initiation and total breakup time can be calculated. For example, assuming a 60 μm droplet moving with 100 m/s in a stagnant air environment, then the initiation breakup time is 0.017 ms and the total breakup time is 0.07 ms. The relaxation time of a 60 μm droplet is 8.9 ms (table 3) which is very large relative to the breakup time. Hence the measured velocities of the 60 μm droplets over the timescales of this experiment, namely 4 ms, closely correspond to those prevailing at the time of generation of this size.